IEEE Access
Multidisciplinary | Rapid Review | Open Access Journal

Received December 21, 2020, accepted January 4, 2021, date of publication January 11, 2021, date of current version January 25, 2021.

Digital Object Identifier 10.1109/ACCESS.2021.3050511

Design of Full-Order State Observer for Motor Drive Systems Based on the Fixed Gain Filter

CAN WANG[1], WEINAN WU[2,4], GUOCHONG LI[1], GUILIN YANG[3], (Member, IEEE), CHI ZHANG[3], (Senior Member, IEEE), AND JIANFEI PAN[1], (Member, IEEE)

[1]College of Mechatronics and Control Engineering, Shenzhen University, Shenzhen 518061, China
[2]Beijing Institute of Specialized Machinery, Beijing 100143, China
[3]Ningbo Institute of Materials Technology and Engineering, Chinese Academy of Sciences, Ningbo 315201, China
[4]College of Intelligent Systems Science and Engineering, Harbin Engineering University, Harbin 150001, China

Corresponding author: Jianfei Pan (pan_jian_fei@163.com)

This work was supported in part by the National Natural Science Foundation of China under Grant U1913214 and Grant 52007121, in part by the Guangdong Provincial Natural Science Foundation under Grant 2019A1515012165, and in part by the General Research Project of Shenzhen Science and Technology Plan under Grant JCYJ20190808113009469.

ABSTRACT This paper mainly discusses about the full-order state observation technology for the permanent magnet synchronous motor (PMSM) drive system. First, the concept of the Kalman filter (KF) is synthesized to design a novel fixed gain filter (FGF) with an optimal fixed feedback gain matrix, which ensures a fast and accurate observation for position, speed, acceleration, and load torque. To alleviate the heavy computational load of the KF, second, the feedback gain is configured as a single tunable parameter only, which can be calculated offline. The regulation parameter is refined within a certain small range by fulfilling the system stability criterion. Furthermore, the system dynamic performance indexes, such as noise smoothing capability and bandwidth, are both analyzed to deduce the expected exact value of the regulation parameter. The proposed FGF can provide an accurate observation equivalent to the conventional KF, while the proposed FGF provides a faster tracking performance, an easier parameter tuning mechanism, and a lower program complexity. The performance of the FGF is verified by simulations and experiments in all cases.

INDEX TERMS Permanent magnet synchronous motor (PMSM), fixed gain filter (FGF), motor drive, state estimation, load torque observation.

I. INTRODUCTION

The permanent magnet synchronous motor (PMSM) is widely applied in high-performance control fields such as computerized numerical control machine tools, medical instruments, and aerospace, etc., owing to its high power factor and good speed control performance. For the PMSM servo closed-loop control system, the rotor position is the necessary feedback signal for accurate vector control. In actual operation, however, external factors such as load fluctuations and parameter changes often adversely affect the position control precision [1], [2]. Therefore, the knowledge of state quantities information such as motor position, speed, load torque, etc., are essential to achieve a high dynamic performance of a PMSM.

The associate editor coordinating the review of this manuscript and approving it for publication was Yang Tang.

In traditional position measurements, the position signal is usually obtained by an optical encoder. On this basis, the speed signal is often calculated by the differential calculation from M method, T method and M/T method [3]. In order to suppress the influence of external interference on the system, the scheme of load torque observation is usually studied based on the measured position and speed signals [4]. However, on one hand, the factors that imperfect manufacturing, quantization noise of the optical encoder will cause measurement errors of the rotor position; on the other hand, the traditional speed measurement method often causes time delay and speed error, termed as speed noise [5]. For the existence of measurement noise and speed noise, the accuracy of the load torque observation is hard to be guaranteed. As a result, the dynamic performance and stability of the PMSM servo system can often be affected [6]. Although low-pass filters are usually adopted to suppress different kind of noise, they cannot reduce time delay simultaneously [7]–[9].

The high-precision encoders succeed in the improvement of measurement accuracy, however, the cost is high, and their size, weight, wiring complexity will reduce the mechanical strength and reliability of the entire PMSM control system.

To overcome the problems from traditional sensor and encoder measurement methods, in recent years, numerous state observation technologies have been perused for motor drive systems [10]–[12]. The most widely used observation methods include: Luenberger observer (LO) [13], [14] and Kalman filter (KF) [15], [16].

For the sensorless linear induction motor drive system, a neuron-based full-order Luenberger adaptive speed observer is proposed in [17], and the speed is estimated. An improved sliding mode Luenberger state observer is proposed in [18], which is employed to estimate the rotor speed and disturbance torque. By limiting the sliding surface of the estimated interference and stator current error, the interference suppression mechanism is designed that can reduce the influence of the external load on the tracking performance of the observer. In [19], an adaptive non-singular terminal sliding mode control based on Luenberger disturbance observer is carried out, which can quickly track load torque and external disturbances. In [20], a minimum-order observer is introduced to estimate the load disturbance, which is further implemented for PMSM predictive control. With this scheme, rapid tracking, stability, and disturbance suppression performances are achievable.

In practice, LO is only suitable for linear systems with constant parameters and low measurement noise [21]. For systems that are interfered by measured noise and accompanied by variable parameters, however, KF possesses better performance with the intrinsic characteristics of direct reliance of measurement noise, which makes KF extensively applied as an optimal state estimator [22], [23].

In [24], a large number of applications and implementation issues of KF in trajectory estimation, state control or diagnosis, parameter estimation, data merging, signal processing, etc., are summarized. Considering the noise of speed measurement, a new scheme that combines speed and load torque on-line observation is proposed in [25]. The disturbance is estimated by KF, and in turn, the observed load torque is employed to compensate for the speed fluctuations caused by the load disturbance. In [26], KF is adopted to estimate the unknown disturbances of robot joint motors in noisy environments. In [27], KF is applied as an observer for rotor position, speed and load torque information. On this basis, the observations are compensated for the predictive functional controller, and the results prove the effectiveness of the algorithm in speed detection and interference suppression [28]. An adaptive Kalman observer for position, speed and load torque is proposed in [29] for PMSM servo system, which can effectively alleviate the problem of large speed error and time delay at low speed. In order to reduce the lateral dynamic impact caused by the mechanical backlash of the independently-driven dual-motor electric vehicle, KF is employed to design a dynamic smoothness controller in [30]. The impact of process noise on the control performance is discussed as well.

Obviously, KF is an effective way to solve the problems of sensor quantization error and measurement noise. However, on one hand, it is difficult to correctly set the initial values of the covariance matrixes of KF, which usually requires certain amount of trial and error; on the other hand, the complex real-time computation process of KF greatly limits its vast use in practical applications. Many improvements have been performed to address this issue. Based on the KF principle, the fixed gain filter (FGF) is studied in [31]–[34], which is applied to observe system position, speed and acceleration signals for tracking and scanning. Compared with KF, FGF can greatly reduce the computation complexity and ensure the accuracy of observation. In the study [35] and [36], the FGF is applied for grid synchronization technology. In comparison to the traditional phase-locked loop approach, it is easy to adjust parameters and can provide faster and more accurate grid angle and frequency information.

Motivated by the above observations, a new FGF-based full-order state observer of the PMSM drive system is proposed. The synthesis of FGF-based full-order state observer is a first attempt on motor drive systems, and the ultimate goal of the work is to observe position, speed, acceleration, and load torque accurately and fast with an easy parameter tuning mechanism and a low computational burden.

The major contributions of this paper include the following.

1) Based on the fixed gain theory of KF, an FGF full-order state observer model for the motor drive system is constructed, which can observe position, speed, and load torque.

2) Two dynamic characteristics indexes, noise filtering and bandwidth, are analyzed. By weighing the tradeoff between the both indexes, the expected regulation parameter can be determined for the expected observation performance.

The paper is organized as follows. The mathematical model of the motor drive system is presented in Section II. The theory and design of the full-order observer based on the PMSM drive system are formulated in Section III. The performance analysis and parameter regulation mechanism of the observer are studied in Section IV. Experimental results are given in Section V, followed by Section VI which concludes this paper.

II. MODEL OF MOTOR DRIVE SYSTEMS

PMSM servo drive systems mainly apply the field-oriented control to realize closed-loop control of current, speed and position loop. Ignoring the elasticity of the transmission, the motor drive system can be modeled as a one-mass rigid system. The electromagnetic torque T_e and the load torque T_L act together on the inertia-damping body with moment of inertia J and damping b, to determine motor position θ, speed ω and acceleration a. The equivalent motion system behavior

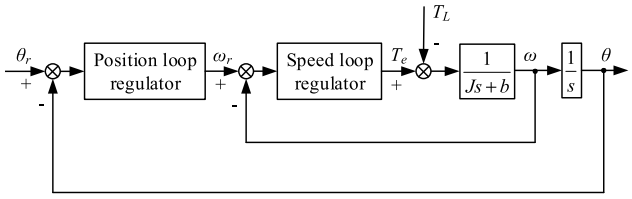

FIGURE 1. Block diagram of the PMSM drive system.

can be represented as the following differential equation:

$$\begin{cases} Ja = T_e - b\omega - T_L \\ a = \ddot{\theta} \\ \omega = \dot{\theta} \end{cases} \tag{1}$$

In general, the bandwidth of the current loop is much greater than that of the speed loop, so the current loop is usually simplified to 1. The simplified block diagram of the PMSM drive system is shown in Fig. 1.

III. DESIGN OF THE FULL-ORDER STATE OBSERVER BASED ON THE FIXED GAIN FILTER THEORY

A. THIRD-ORDER FIXED GAIN FILTER

The third-order FGF derives the optimal gain matrix based on the principle of the steady state KF. Its special form is derived step by step from the mutual derivative relationship of the state matrix elements [34]. As a result, the state matrix $\boldsymbol{x} = [\theta\ \omega\ a]^T$ is usually selected for system modeling. Therefore, the state equation of third-order observer for the rotary motion system is established as:

$$\begin{cases} \mathbf{x}(k+1) = \mathbf{F}\mathbf{x}(k) + \mathbf{\Gamma}\mathrm{w}(k) \\ \mathbf{y}(k) = \mathbf{H}\mathbf{x}(k) + \mathbf{v}(k) \end{cases}$$
$$\mathbf{F} = \begin{bmatrix} 1 & T & T^2/2 \\ 0 & 1 & T \\ 0 & 0 & 1 \end{bmatrix}, \quad \mathbf{H} = \begin{bmatrix} 1 & 0 & 0 \end{bmatrix}, \quad \mathbf{\Gamma} = \begin{bmatrix} T^2/2 \\ T \\ 1 \end{bmatrix} \tag{2}$$

where $\mathbf{x}$ and $\mathbf{y}$ are the state variables and measurement outputs, respectively, $\mathbf{F}$ is the state-transition matrix, $\mathbf{\Gamma}$ is the process noise transition matrix, and $\mathbf{H}$ is the observation matrix that maps the state variable into the observed variable. T is the sampling period.

The process noise $\mathbf{w}(k)$ and measurement noise $\mathbf{v}(k)$ are zero-mean white noise sequences with the covariance matrices defined as

$$E\left\{\mathbf{w}(k)\,\mathbf{w}(k)^T\right\} = \sigma_w^2\ E\left\{\mathbf{v}(k)\,\mathbf{v}(k)^T\right\} = \sigma_v^2 \tag{3}$$

The iterative algorithm of KF is shown in (4), where superscript $\sim$ means the predicted value, and ^means the observed value. The optimal Kalman gain $\mathbf{K}(k)$ can be derived by minimizing the covariance $\mathbf{P}(k)$. It can be seen that KF solves the gain matrix in real time, which leads to a large amount of calculation.

$$\begin{cases} \tilde{\mathbf{x}}(k) = \mathbf{F}\hat{\mathbf{x}}(k-1) \\ \tilde{\mathbf{P}}(k) = \mathbf{F}\hat{\mathbf{P}}(k-1)\,\mathbf{F}^T + \mathbf{\Gamma}\sigma_w^2\mathbf{\Gamma}^T \\ \mathbf{K}(k) = \tilde{\mathbf{P}}(k)\,\mathbf{H}^T\left[\mathbf{H}\tilde{\mathbf{P}}(k)\,\mathbf{H}^T + \sigma_v^2\right]^{-1} \\ \hat{\mathbf{x}}(k) = (\mathbf{I} - \mathbf{K}(k)\,\mathbf{H})\,\tilde{\mathbf{x}}(k) + \mathbf{K}(k)\,y(k) \\ \hat{\mathbf{P}}(k) = (\mathbf{I} - \mathbf{K}(k)\,\mathbf{H})\,\tilde{\mathbf{P}}(k) \end{cases} \tag{4}$$

According to the operation mechanism of KF, the optimal gain matrix is obtained as KF reaches a steady state. At this time, the error covariance matrix $\tilde{\mathbf{P}}(k)$ and $\hat{\mathbf{P}}(k)$ both have converged to a stable state, so we have,

$$\tilde{\mathbf{P}}(k) = \tilde{\mathbf{P}}(k-1)\ \hat{\mathbf{P}}(k) = \hat{\mathbf{P}}(k-1) \tag{5}$$

The optimal fixed gain matrix form of the third-order FGF can be further derived as follows [29],

$$\mathbf{K}(k) = \begin{bmatrix} \alpha & \dfrac{\beta}{T} & \dfrac{2\gamma}{T^2} \end{bmatrix}^T \tag{6}$$

where α, β, and γ are dimensionless constants, which can actually be solved in an analytic form, and the solution can be expressed in one parameter. The so-called noise filtering index, which is the ratio of the motion to the observation uncertainties, is defined as

$$\lambda = \frac{T^2\sigma_w}{\sigma_v} \tag{7}$$

$$\begin{cases} \lambda = \dfrac{2\gamma}{\sqrt{1-\alpha}} \\ \gamma = \dfrac{\beta^2}{4\alpha} \\ \beta = 4 - 4\sqrt{1-\alpha} - 2\alpha \end{cases} \tag{8}$$

From (8), all the feedback gains of the FGF are in relation to λ. Once this parameter is evaluated, the optimal steady-state gain parameters α, β, and γ, as well as the resulting performance, are specified in advance.

In summary, FGF corresponds to the optimal gain matrix of the steady-state KF. The elements in $\mathbf{K}(k)$ are all constant values and fixed gains, therefore, the real-time calculation amount of KF can be greatly reduced.

B. FGF-BASED STATE OBSERVER MODEL OF MOTOR DRIVE SYSTEMS

The FGF model can be established according to the operating law of the rotating electrical machine system, as shown in (9). The directly observed state variables include: motor position $\hat{\theta}$, speed $\hat{\omega}$, and acceleration $\hat{a}$.

The motor driver obtains T_e in real time by measuring the current feedback through the current sensor. With this property, the load torque $\hat{T}_L$ can be obtained indirectly through the observation of acceleration and speed, as shown in (10),

$$\begin{cases} \tilde{\theta}(k) = \hat{\theta}(k-1) + T\hat{\omega}(k-1) + \dfrac{T^2}{2}\hat{a}(k-1) \\ \tilde{\omega}(k) = \hat{\omega}(k-1) + T\hat{a}(k-1) \\ \tilde{a}(k) = \hat{a}(k-1) \end{cases} \tag{9}$$

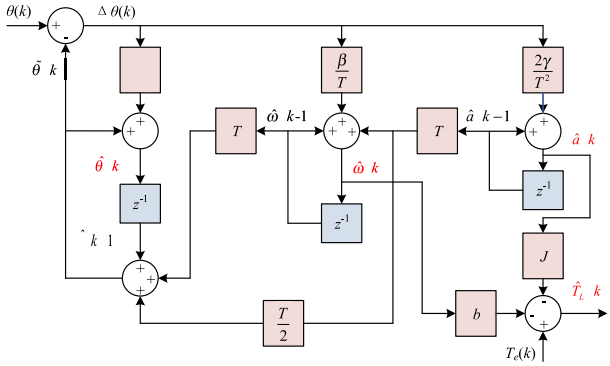

FIGURE 2. Block diagram of the FGF-based State Observation of motor drive systems.

$$\hat{T}_L(k) = T_e(k) - b\hat{\omega}(k) - J\hat{a}(k) \tag{10}$$

The motor position θ measured by the encoder can correct the observation values in real time, thereby continuously improving the observation precision of the observer. The difference between the measured and predicted position $\Delta\theta(k)$ is used as the input of the FGF. The full-order state observation structure of the PMSM drive system based on the proposed FGF is shown in Fig. 2.

IV. OBSERVATION PERFORMANCE ANALYSIS AND PARAMETER DESIGN OF THE FGF-BASED OBSERVER

It can be seen from (7) and (8) that, although all gain matrix parameters can be represented by λ, λ is related to σ_v, which is difficult to directly observe, so the adjustment process is not easy. In order to simplify the tuning process, an adjustable parameter κ uniquely related to λ is derived. The range of the tunable parameter of the observer can be narrowed by analyzing the stability of the FGF. Furthermore, through analyzing the dynamic characteristics of the FGF, the function of two indicators of noise filtering and observation speed can be established. According to the compromise between the two indicators, the expected parameter can be determined corresponding to the best observation performance. Therefore, through the analysis of the observer performance in this section, the problem of complex parameter adjustment process and difficult parameter setting is transformed into a subjective design of observer performance, thereby greatly simplifying the adjustment process.

A. STABILITY ANALYSIS

In order to further simplify the calculation process, the regulation parameter $\kappa = \sqrt{1-\alpha}$ is introduced. At this time, the unique explicit expression of κ corresponding to the optimal gain matrix $\mathbf{K}(k)$ can be obtained, as shown in (11). The range of κ is $\kappa \in (0, 1)$. The performance of FGF can thus be uniquely adjusted according to κ, as recommended in [35].

$$\begin{cases} \alpha = 1 - \kappa^2 \\ \beta = 2(\kappa - 1)^2 \\ \gamma = (1-\kappa)^3 \Big/ (\kappa + 1) \end{cases} \tag{11}$$

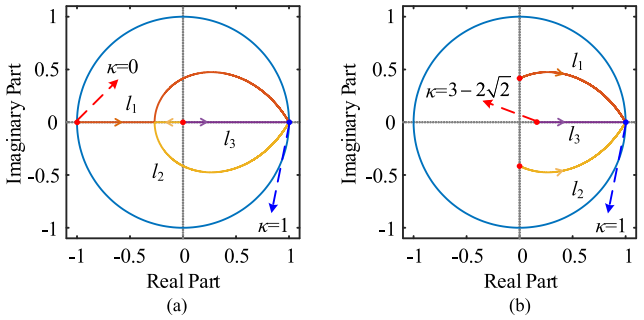

FIGURE 3. Root locus of discrete FGF (a) $\kappa \in (0,1)$. (b) $\kappa \in (3-2\sqrt{2}, 1)$.

In order to facilitate the adjustment of FGF, the tunable range of κ is primarily reduced according to the stability of FGF. Since the stability of the observer is only related to the poles of the system, the system is stable only when all the poles are in or on the unit circle. Meanwhile, the zeros affect the amplitude and phase of the system unit impulse response. Therefore, the range of κ can be optimized according to the configuration of pole position.

From (4), the relationship between the state matrix and the system output is as follows,

$$\hat{\mathbf{x}}(k) = [z\mathbf{I} - (\mathbf{I} - \mathbf{K}(k)\mathbf{H})\mathbf{F}]^{-1}\mathbf{K}(k)zy(k) \tag{12}$$

The transfer function from the measured position to the observed position can thus be derived as shown in (13), and the characteristic equation $D(z)$ is shown in equation (14). It can be seen from (13) that when the system enters a steady state (z equals to 1), there is $G_\theta = 1$. Thus, no matter what form the given position signal can be, its observation value will track the command completely without error.

$$G_\theta = \frac{\hat{\theta}(k)}{\theta(k)} = \frac{\left(\kappa^3+\kappa^2-\kappa-1\right)z^3+\left(-3\kappa^3-3\kappa^2+7\kappa-1\right)z^2+\left(4\kappa^3-4\kappa^2\right)z}{D(z)} \tag{13}$$

$$D(z) = (-\kappa-1)z^3 + (7\kappa-1)z^2 + \left(\kappa^3 - 7\kappa^2\right)z + \left(\kappa^3+\kappa^2\right) \tag{14}$$

From (14), the root locus of the system can be depicted as Figure 3(a), where l_1, l_2, and l_3 represent the trajectories of the three closed-loop poles respectively, when κ changes from 0 to 1.

In order to make the discrete system possess a better dynamic performance, it is expected that all the poles of the closed-loop pulse transfer function have the following distributions:

1) To make the system stable, the closed-loop poles should be distributed in the unit circle;

2) To make the transient process of the system smooth (less oscillations), the closed-loop poles should lie on the right half plane of the unit circle.

According to the above analysis, the root locus shown in Fig. 3(a) for $s \in (0, 1)$ evolves into the corresponding

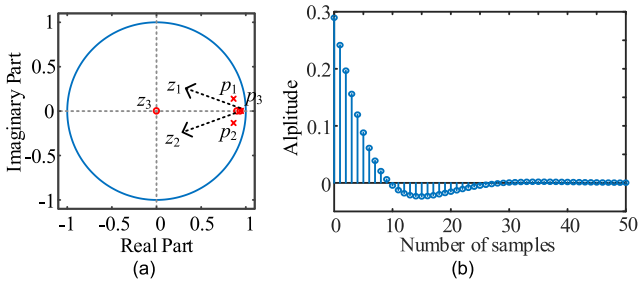

FIGURE 4. Zero-Pole position and system characteristics of the FGF-based observer ($\kappa = 0.84$) (a) Pole-zero position. (b) Impulse response.

closed-loop pole position with $\kappa \in \left(3-2\sqrt{2}, 1\right)$, as depicted in Fig. 3(b). Actually, for the pole location of the FGF, the closer the pole approaches to the unit circle, the longer is the transient response time. Conversely, the greater distance to the unit circle means a faster transient response yet more severe noise.

Fig. 4(a) shows the positions of the zeros (z_1, z_2, and z_3) and the poles (p_1, p_2, and p_3) of the transfer function (13) at $\kappa = 0.84$. It can be observed that the system contains three poles that lie in the unit circle, so this system is stable. Likewise, the system contains three zeros. Because there is a zero located at $z = 0$, it only affects the phase-frequency characteristics but does not affect the amplitude response. Fig. 4(b) shows the unit impulse response of the system with a sampling rate of 1/50. Obviously, the impulse response curve converges as the number of samples increases, indicating that FGF is a causally stable system. In fact, as long as the value of κ is selected within the stable range, the causal stability of the system can be proved, that is, the system is physically achievable. Moreover, different values of κ will affect the response performance of the system, that is, the smaller κ is, the faster the response but the larger the overshoot of the corresponding system will be. While the larger κ is, the longer the stable time but smoother of the corresponding system becomes.

Based on the stability or the impulse response of the proposed FGF analyzed above, the range of κ is initially determined. As a tradeoff between the noise sensitivity and tracking capability, the value of κ can be achieved by the desired system performance design within the stability range.

In order to further clarify the exact value of κ, the functional relationship between the dynamic performance indexes and κ should be established. The adjustment mechanism of κ can further be obtained on account of the expected system performance.

B. DYNAMIC CHARACTERISTICS ANALYSIS

In order to determine the exact κ in the stable region, the quantitative relationships between κ, the noise index, and the bandwidth index are studied respectively.

1) NOISE FILTERING INDEX λ

The observer should have the ability to suppress noise. In the controlled system, there are usually two forms of noise, one is process noise $w(k)$ and the other is measurement noise $v(k)$. $w(k)$ is often related to the rounding error of the computation, the degree of model linearization, and the discretization error. $v(k)$ is often related to the position sensor precision, which is settled as the system hardware is fixed. Therefore, λ shown in (7) can be used to describe the noise filtering parameter. The larger λ is, the greater the noise but the worse the filtering ability will be. While the lower λ is, the weaker the noise and the stronger the filtering ability can be declared.

Although it can be seen from (7) that λ is usually a fixed parameter, it is still expected that the observer can be designed according to the needs of the observer user, for example, the expected noise filtering parameter index λ^*. Indeed, it can be deduced that κ can be expressed in terms of λ only. Therefore, the relationship is established in (15), where the corresponding expected parameter κ_1^* can be calculated according to λ^*, so as to achieve an ideal observation performance.

$$\kappa_1^* = \frac{\sigma}{6} - \frac{\lambda^*}{6} + \frac{\lambda^*\left(\lambda^* - 18\right)}{6\sigma} + 1$$
$$\sigma = \sqrt[3]{27\lambda^{*2} - 108\lambda - \lambda^{*3} + 3\lambda\sqrt{1296 - 3\lambda^{*2}}} \tag{15}$$

From (15), a monotone decreasing interdependence relationship can be deduced between κ_1^* and λ^* within the domain of definition. Since λ^* is greater than and close to 0, when the measurement error is fixed, the smaller λ^* is, the better the noise filtering effect becomes.

2) OBSERVER BANDWIDTH INDEX ω_b

In practical applications, the target trajectory is usually time-variant. Therefore, the observer should also maintain a fast and accurate observation performance. This indicator can be characterized by the observer bandwidth ω_b. The larger the bandwidth is, the faster the tracking target and the smaller the tracking error becomes. Since bandwidth is a frequency domain characteristic, the s-domain transfer function that corresponds to (13), can be calculated by the bilinear discretization method. Then the function of the expected κ_1^* and the expected ω_b^* can be calculated by

$$20\lg\left|G_\theta(z)|z = \frac{1+\frac{j\omega_b^* T}{2}}{1-\frac{j\omega_b^* T}{2}}\right| = -3. \tag{16}$$

Solving (16), we can get that κ_1^* is a sixth-order equation about ω_b^*, and the explicit solution is complicated.

It is worth noting that, κ_1^* is a monotonic decreasing function of ω_b^*. When $\kappa_1^* \in \left(3-2\sqrt{2}, 1\right)$, the bandwidth range is $\omega_b^* \epsilon (0, \infty)$. Nevertheless, the limitation of the sampling period T accounts for the fact that ω_b^* cannot reach ∞. For further taking both the controller bandwidth ω_c and the Shannon's Theorem into consideration, the range of ω_b^* can be refined to $(\omega_c, \pi/T)$, and the design of ω_c varies associated with different observed states.

It can be seen from the above analysis that, considering the limitation of the controller bandwidth and sampling

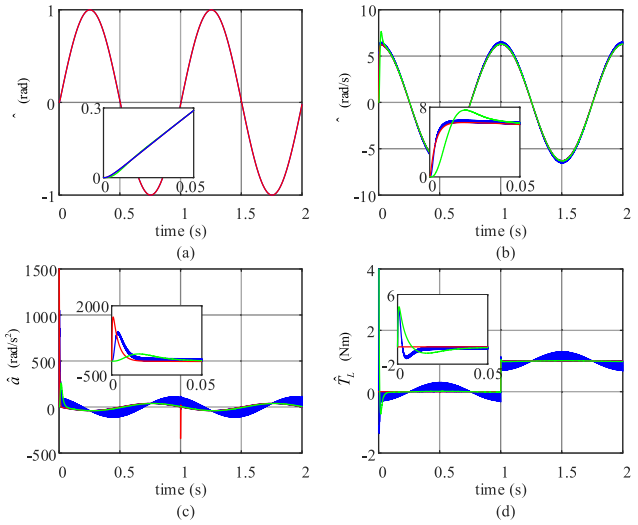

FIGURE 5. Comparison result of FGF observation under sine given position at $\kappa = 0.85$ and $\kappa = 0.98$. (a) position, (b) speed, (c) acceleration, (d) load torque. The red lines stand for the real state, the green lines stand for the observation results under $\kappa = 0.98$, and the blue lines stand for the observation results under $\kappa = 0.85$.

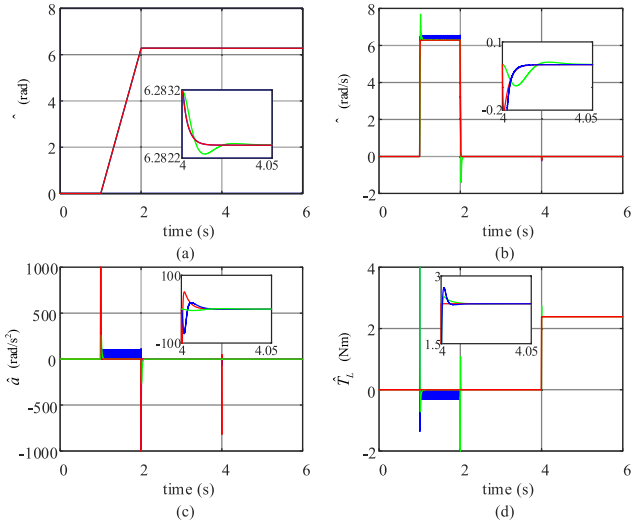

FIGURE 6. Comparison results of FGF observation at $\kappa = 0.85$ and $\kappa = 0.98$ under given step position. (a) position, (b) speed, (c) acceleration, (d) load torque. The red lines stand for the real state, the green lines stand for the observation results under $\kappa = 0.98$, and the blue lines stand for the observation results under $\kappa = 0.85$.

frequency in practical control systems, the range of κ is further reduced.

C. SIMULATION VERIFICATION

The parameters of the simulations are set as: $T = 10^{-4}$ s, and the electromagnetic torque limit is twice of the rated torque. The proportional-integral (PI) controller parameters of the speed loop are $k_p = 10$, $k_i = 0.01$, with the bandwidth configured as about 550 Hz. The parameter of the position loop proportional (P) controller is $k_{pp} = 300$, and the bandwidth is around 52 Hz. Fig. 5 and Fig. 6 show the comparison results of the observation results with different

TABLE 1. Observation state tracking time during motor startup.

Tracking time (ms)	Sine position command		Slope position command	
	K=0.85	K=0.98	K=0.85	K=0.98
Position	0	0	0	0
Speed	24	37	10	13
Acceleration	30	36	35	45
Load torque	22	30	38	83

κ under different position references, respectively. In the figures, the red line stands for real state, the green line stands for the observation results under $\kappa = 0.98$, and the blue line stands for the observation results under $\kappa = 0.85$.

A test case involving a position sinusoidal with the amplitude 1 rad and the frequency 1 Hz is considered. The 1 N·m load torque step occurs at 1 s. The comparison results of observations at $\kappa = 0.98$ and $\kappa = 0.85$ are shown in Fig. 5. From Fig. 5, the proposed FGF has a high observation accuracy of position, speed, acceleration and load torque. As the load torque observation model involves speed and acceleration, the error is increased. It can be seen from the enlarged figure from 0 to 0.05 s that, as κ increases, the observation noise becomes smaller, however, the tracking speed becomes slower, which is consistent with the theoretical analysis.

The observation results with a ramp given position (the slope and amplitude are both 2π) under $\kappa = 0.98$ and $\kappa = 0.85$ are shown in Fig. 6. Half rated load is suddenly added as the load torque at 4 s. The proximities between the observation and real values are evident, which confirms the superior performance of the FGF. At 4 s, the torque output is insufficient due to the load, resulting in a slight drop of 0.001 rad. Additionally, the waveforms from 4 s to 4.05 s are expanded, to observe the observation performance when the sudden load is added. It can be seen that when κ increases, the observation noise decreases, however, the bandwidth also decreases that results in a slow observation speed, which is consistent with the above theoretical analysis.

D. QUANTITATIVE ANALYSIS OF SIMULATION RESULTS

In order to evaluate the performance of the observer, Table 1 summarizes the time required for accurate observation of each state to track the actual value during the startup phase (begins at 0 s for sine given and 2 s for slope given) in Fig. 6. It can be seen that the observation speed of each state at $\kappa = 0.98$ is slower than that at $\kappa = 0.85$.

In order to analyze the sensitivity of FGF, the root mean square error (*RMSE*) generated from the state observation difference, is calculated as the performance metric and it is defined as (17).

$$RMSE = \sqrt{\frac{\sum_{k=1}^{n} \left(\hat{x}_k - x_k\right)^2}{n}} \tag{17}$$

TABLE 2. *RMSE* calculated after loading to approaching steady state.

RMSE	Sine position command		Slope position command	
	K=0.85	K=0.98	K=0.85	K=0.98
Position	1.95 e-4	1.83 e-4	4.82 e-4	2.72 e-4
Speed	10.69 e-2	1.78 e-2	9.30 e-3	0.27 e-2
Acceleration	43.86	3.36	37.70	0.14
Load torque	12.76 e-2	0.98 e-2	8.27 e-2	0.04 e-2

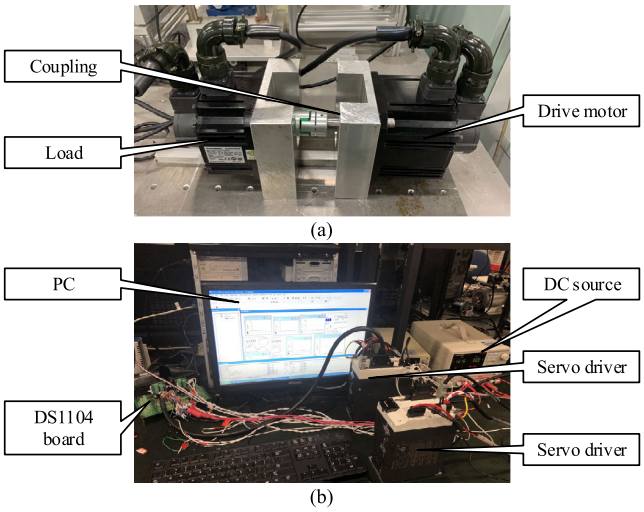

FIGURE 7. The experimental setup. (a) Motor drive mechanical setup, (b) Control platform.

From the simulation results in Fig. 6, as the servo system is in steady state after loading (begins at 1 s for sine given and at 4 s for slope given), we can calculate the *RMSE* as shown in Table 2. It is evident that the observation error of each state at $\kappa = 0.98$ is less than that at $\kappa = 0.85$. The accuracy of position tracking is the highest, but the accuracy of acceleration is the lowest for the two differential calculation.

V. EXPERIMENTAL VERIFICATION RESULTS

A. EXPERIMENTAL SETUP

In order to verify the effectiveness of the proposed FGF, an experimental setup has been implemented, which is presented in Fig. 7. It is composed of two Panasonic©MINAS A6 series PMSM motors, one of which is MDMF 102L1G6M as the driver and the other is MHMF 102L1G6M as the load machine. An 1kW Panasonic©MDDLT45SF driver is used to control the motors. The two motors are coupled by a NBK©rigid coupling. The direct current (DC) buses of the driver motor and the load motor are in parallel connection and the load motor is used as a generator to supply the load torque. The position of the driving motor are measured by an incremental encoder, and the speed and acceleration are calculated by differentiation process through the measured position. The main parameters are presented in Table 3.

TABLE 3. Main parameters of PMSM drive system.

Parameter	Nominal value
Motor power	1 kW
Motor torque	4.77 N·m
Motor speed	2000 r/min
Inertia of motor	$6.18*10^{-4}$ N·m^2
Inertia of load	$22.9*10^{-4}$ N·m^2
Encoder resolution	23 bit

Experimental validation of the proposed FGF scheme is constructed on MATLAB/Simulink environment and compiled and executed on dSPACE DS1104 real-time controller board. The sampling time is set to 1 ms.

B. EXPERIMENTAL RESULTS

Through the command position, the position, speed, acceleration, and load toque act as the observed states implementing with the proposed FGF. Among them, because the load torque observation model involves system damping, the damping should be treated as a prior parameter. It is approximately 0.007 N·m·s/rad, which is calculated by the relationship between the electromagnetic torque and speed under speed loop without load. The effectiveness of the proposed FGF is assessed in Fig. 8, Fig. 9, and Fig. 10, respectively.

Fig. 8 presents the observation results commanded by a ramp position with both amplitude and slope of 2π, and half the rated load added after 3 s. A drop of 0.024 rad after loading could be observed in the Fig. 8 (a) and Fig. 8 (e). From Fig. 8 (b) and Fig. 8 (f), since the differential processing of the position feedback, when the position slope has a turning point, the speed and acceleration feedback have spikes and noise. On the other hand, position feedback is used as an FGF input that has a direct impact on the observation results, which is manifested as a sharp peak on the observation results when the position slope appears a turning point. However, it does not affect the noise smoothing ability of the observer, which is only related to parameter κ. By comparing the actual value with the observation result, it can be concluded that the larger κ, the stronger the noise suppression and the slower tracking capability.

A test case involving a sinusoidal position with the amplitude of 1 rad and frequency of 1 Hz is considered. The observed results are shown in Fig. 9, and Fig. 9 (a)-(d) and (e)-(h) depict the cases $\kappa = 0.98$ and $\kappa = 0.85$ respectively. A sudden change of 30% rated load is added at 2 s.

As evident in Fig. 9 (a) and Fig. 9 (e), the position reference, position feedback and position observation almost coincide, indicating the high accuracy of both the control and observation performance. In Fig. 9 (b), a small deviation between the speed observation and speed feedback can be detected with the lag of approximate 30 ms. By comparing Fig. 9 (c) and Fig. 9 (g), it can be seen that the acceleration

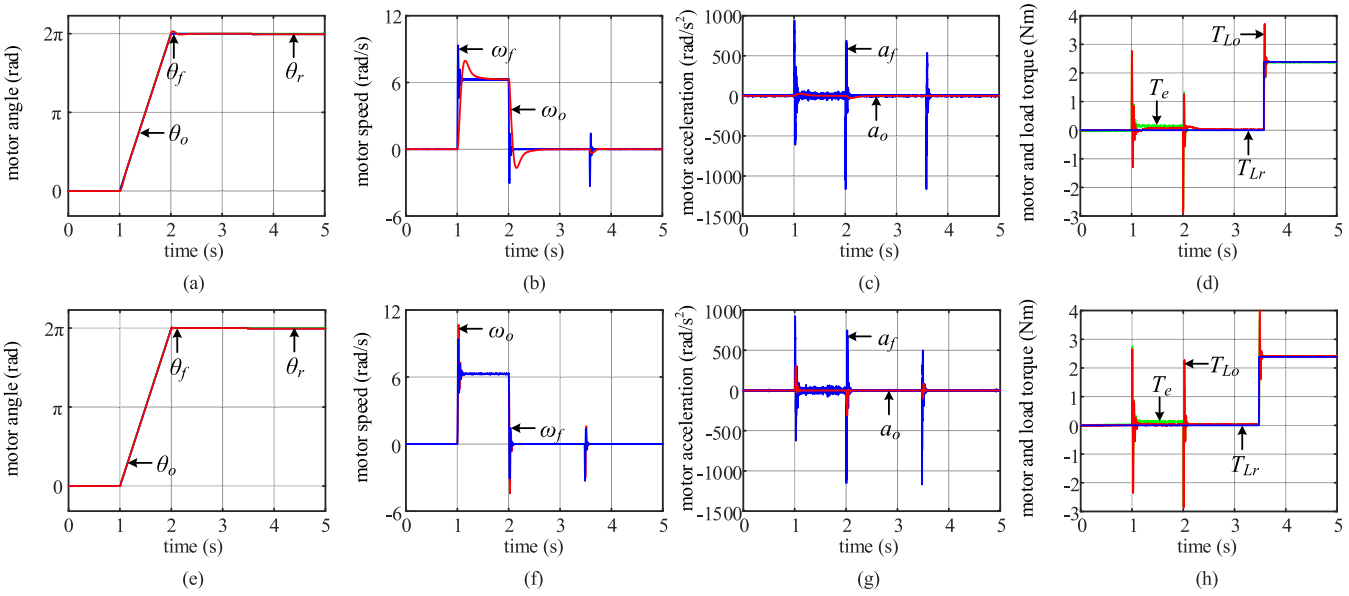

FIGURE 8. Comparison experimental results under given slope position. (a)-(d) for $\kappa = 0.98$, and (e)-(h) for $\kappa = 0.85$. Blue line stands for actual value, red line stands for observed value, and green line stands for reference value.

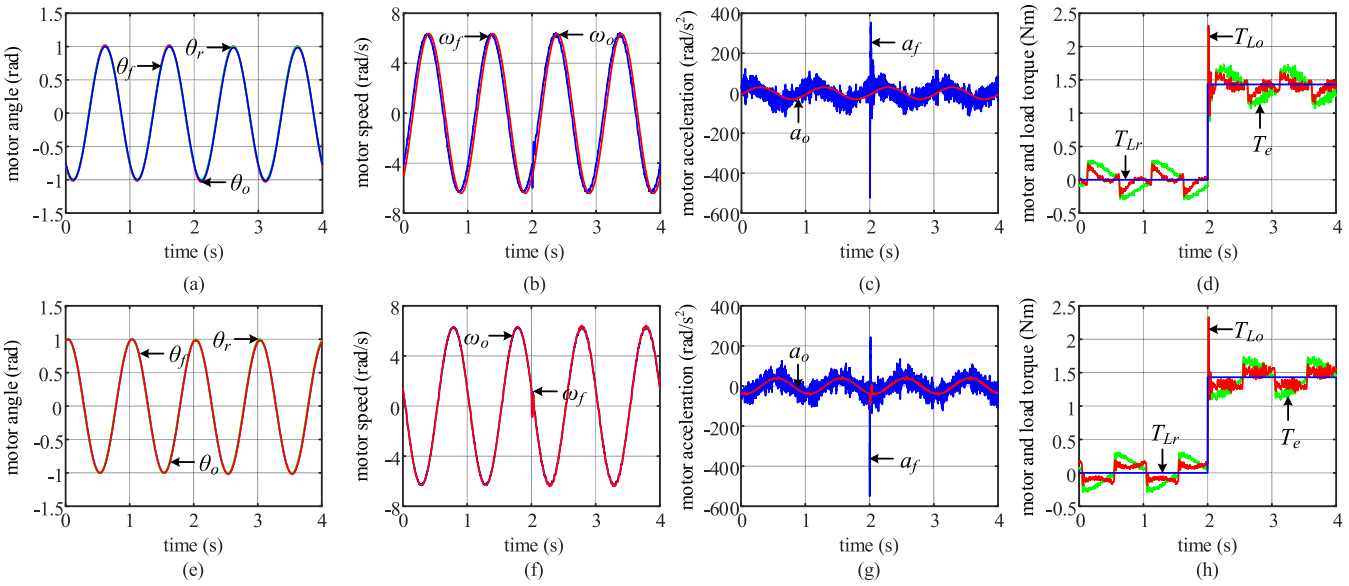

FIGURE 9. Comparison experimental results under given sine position (1Hz). (a)-(d) for $\kappa = 0.98$, and (e)-(h) for $\kappa = 0.85$. Blue line stands for actual value, red line stands for observed value, and green line stands for reference value.

feedback is seriously affected by the noise produced by the second differential of the position. Moreover, when $\kappa = 0.98$, the acceleration observation result has a serious lag, about 165 ms. Nevertheless, the noise smoothing ability is better in comparison to the case of $\kappa = 0.85$. The observation results of the load torque are shown in Fig. 9 (d) and Fig. 9 (h), from which the observation value fluctuates stably around the given value. The observed load torque is close to but slightly lower than the electromagnetic torque, the reason for which is the small inertia and damping in the load torque observation model. In addition, a spike can be detected in the load torque observation at the loading point.

In order to further verify the observation performance, experiments are carried out under the conditions of a sinusoidal frequency of 5 Hz with a sudden load of 1 Nm. As shown in Fig. 10 and Fig. 11, the observation results and the observation error (the difference between the observed value and the true value or the given value) under $\kappa = 0.9$ and $\kappa = 0.7$, are also given. Comparing with Fig. 9, it can be seen that as the frequency of the given position

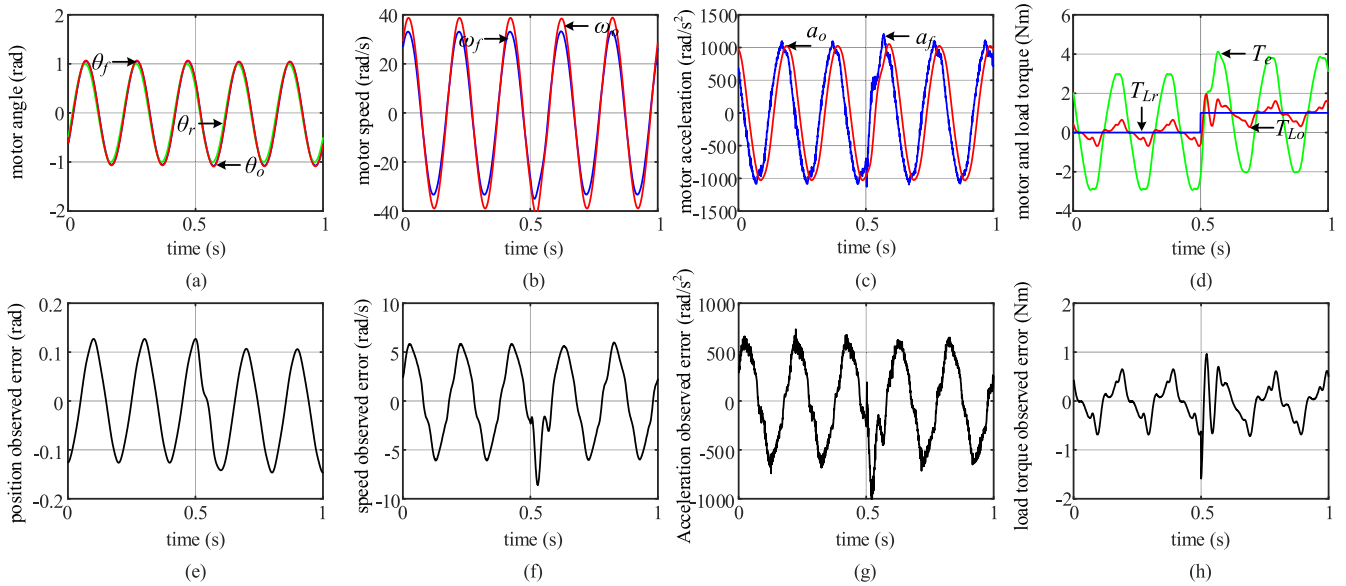

FIGURE 10. Experimental results under given slope position (5Hz) for $\kappa = 0.9$. (a)-(d) the observed states (e)-(h) the observed error. The blue lines stand for actual value, the red lines stand for observed value, and the green lines stand for reference value.

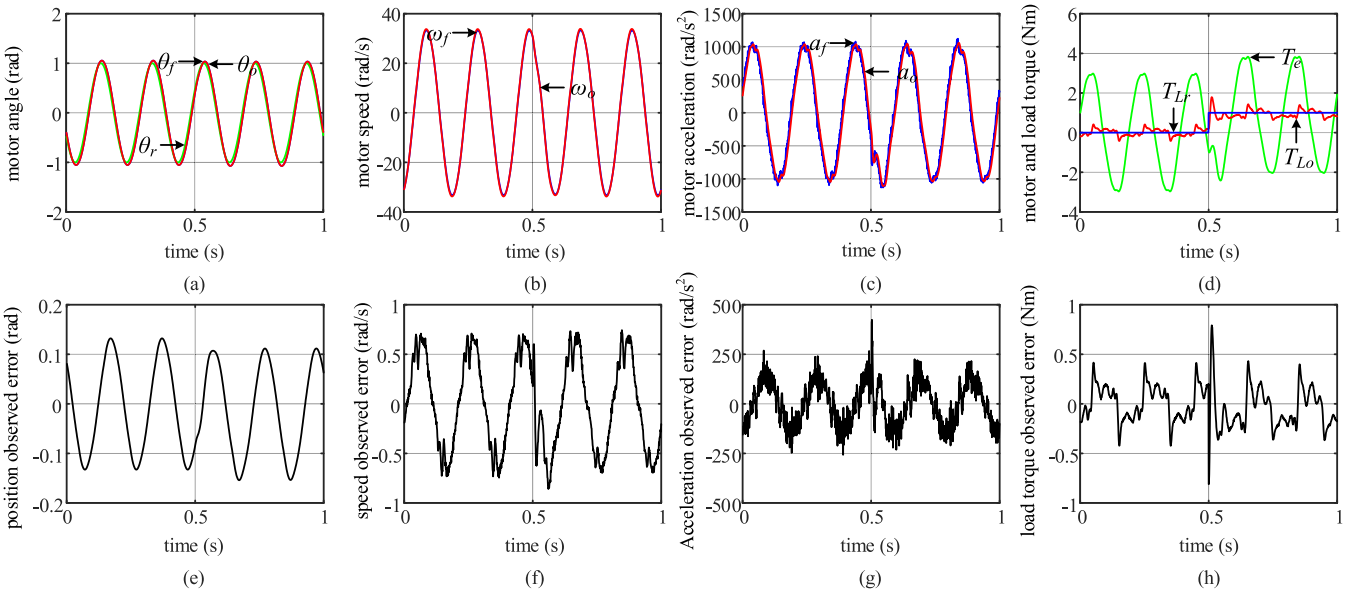

FIGURE 11. Experimental results under given slope position (5Hz) for $\kappa = 0.7$. (a)-(d) the observed states (e)-(h) the observed error. The blue lines stand for actual value, the red lines stand for observed value, and the green lines stand for reference value.

increases, T_e increases significantly. But obviously, when $\kappa = 0.9$, the observed states can no longer keep up with the given or feedback state, and a large observation error occurs. However, as the value of κ decreases as shown in Fig. 11, the tracking speed increases, which greatly reduces the observation error, but the noise increases at the same time. It is worth noting that the observation error is determined by both the observation speed and noise. However, for this case, the observation error is more caused by the low observation speed. The experimental results further illustrate that the value of κ is a trade-off between the tracking speed and the filtering ability, which is consistent with the previous theoretical analysis.

The above experimental results meet rather well with the theoretical analysis and simulation results, which demonstrates the effectiveness of the proposed FGF scheme applied in the PMSM drive system.

VI. CONCLUSION

In this paper, on the basis of the fixed gain KF theory, a new full-order state observer of the motor drive system is proposed. Through the analysis of stability characteristics,

the range of the regulation parameter κ for optimal gain can be narrowed. By analyzing the two dynamic indexes of noise filtering λ and bandwidth ω_b, the adjustment mechanism of κ can be further clarified. We have demonstrated that as κ increases, the observation speed becomes faster, while the noise smoothing ability decreases. As a consequence, it is necessary to make a compromise between both the indexes to decide the expected regulation parameter corresponding to the expected observation performance. Compared with traditional KF, the proposed FGF processes salient features of accurate and fast observation, and reduced complexity performance, which makes it suitable for further study of state feedback control strategies for motor drive systems.

In further work, the influence of the elastic transmission mechanism such as reducer and coupling on the motor drive system can be considered. The FGF for the two-mass system model can also be studied, so as to realize the effective observation of the internal states such as the transmission torque.

REFERENCES

[1] J. Xing, Z. Qin, C. Lin, and X. Jiang, "Research on startup process for sensorless control of PMSMs based on I-F method combined with an adaptive compensator," *IEEE Access*, vol. 8, pp. 70812–70821, Apr. 2020.

[2] K. Qu, W. Li, G. Xu, J. Cao, T. X. Mei, Y. Zhang, and H. Hu, "Rotor-position detection in permanent-magnet wheel motor to ensure smooth startup from standstill," *IEEE Access*, vol. 7, pp. 54179–54191, Apr. 2019.

[3] Y. Chen, M. Yang, J. Long, D. Xu, and F. Blaabjerg, "M/T method based incremental encoder velocity measurement error analysis and self-adaptive error elimination algorithm," in *Proc. 43rd Annu. Conf. IEEE Ind. Electron. Soc. (IECON)*, Oct. 2017, pp. 2090–2805.

[4] Z. Yang, D. Zhang, X. Sun, and X. Ye, "Adaptive exponential sliding mode control for a bearingless induction motor based on a disturbance observer," *IEEE Access*, vol. 6, pp. 35425–35434, Jun. 2018.

[5] M. L. Corradini, G. Ippoliti, S. Longhi, and G. Orlando, "A quasi-sliding mode approach for robust control and speed estimation of PM synchronous motors," *IEEE Trans. Ind. Electron.*, vol. 59, no. 2, pp. 1096–1104, Feb. 2012.

[6] W.-H. Zhu and T. Lamarche, "Velocity estimation by using position and acceleration sensors," *IEEE Trans. Ind. Electron.*, vol. 54, no. 5, pp. 2706–2715, Oct. 2007.

[7] S.-M. Yang and S.-J. Ke, "Performance evaluation of a velocity observer for accurate velocity estimation of servo motor drives," *IEEE Trans. Ind. Appl.*, vol. 36, no. 1, pp. 98–104, Jan. 2000.

[8] R. Petrella, M. Tursini, L. Peretti, and M. Zigliotto, "Speed measurement algorithms for low-resolution incremental encoder equipped drives: A comparative analysis," in *Proc. Int. Aegean Conf. Elect. Mach. Power Electron.*, Sep. 2007, pp. 780–787.

[9] T. Shi, Z. Wang, and C. Xia, "Speed measurement error suppression for PMSM control system using self-adaption Kalman observer," *IEEE Trans. Ind. Electron.*, vol. 62, no. 5, pp. 2753–2763, May 2015.

[10] L. Sheng, W. Li, Y. Wang, M. Fan, and X. Yang, "Sensorless control of a shearer short-range cutting interior permanent magnet synchronous motor based on a new sliding mode observer," *IEEE Access*, vol. 5, pp. 18439–18450, Aug. 2017.

[11] Y. Laamari, K. Chafaa, and B. Athamena, "Particle swarm optimization of an extended Kalman filter for speed and rotor flux estimation of an induction motor drive," *Electr. Eng.*, vol. 97, no. 2, pp. 129–138, Nov. 2014.

[12] T. Tuovinen and M. Hinkkanen, "Signal-injection-assisted full-order observer with parameter adaptation for synchronous reluctance motor drives," *IEEE Trans. Ind. Appl.*, vol. 50, no. 5, pp. 3392–3402, Oct. 2014.

[13] Y. A. Zorgani, Y. Koubaa, and M. Boussak, "MRAS state estimator for speed sensorless ISFOC induction motor drives with luenberger load torque estimation," *ISA Trans.*, vol. 61, pp. 308–317, Mar. 2016.

[14] H. Zoubek and M. Pacas, "Encoderless identification of two-mass-systems utilizing an extended speed adaptive observer structure," *IEEE Trans. Ind. Electron.*, vol. 64, no. 1, pp. 595–604, Jan. 2017.

[15] T. Chen, Y. Cai, L. Chen, X. Xu, H. Jiang, and X. Sun, "Design of vehicle running states-fused estimation strategy using Kalman filters and tire force compensation method," *IEEE Access*, vol. 7, pp. 87273–87287, Jun. 2019.

[16] M. Baykal-Gursoy, "Forecasting: State-space models and Kalman filter estimation," in *Wiley Encyclopedia of Operations Research and Management Sciences*. Hoboken, NJ, USA: Wiley, Jun. 2011.

[17] A. Accetta, M. Cirrincione, M. Pucci, and G. Vitale, "Neural sensorless control of linear induction motors by a full-order luenberger observer considering the end effects," *IEEE Trans. Ind. Appl.*, vol. 50, no. 3, pp. 1891–1904, Jun. 2014.

[18] S. Mohan Krishna and J. L. Febin Daya, "A modified disturbance rejection mechanism in sliding mode state observer for sensorless induction motor drive," *Arabian J. Sci. Eng.*, vol. 41, no. 9, pp. 3571–3586, Jun. 2016.

[19] B. Xu, X. Shen, W. Ji, G. Shi, J. Xu, and S. Ding, "Adaptive nonsingular terminal sliding model control for permanent magnet synchronous motor based on disturbance observer," *IEEE Access*, vol. 6, pp. 48913–48920, Aug. 2018.

[20] S. Wang, J. Fu, Y. Yang, and J. Shi, "An improved predictive functional control with minimum-order observer for speed control of permanent magnet synchronous motor," *J. Electr. Eng. Technol.*, vol. 12, no. 1, pp. 272–283, Jan. 2017.

[21] M. R. Riahi, B. Esmaeilnejad, and F. Tahami, "Speed control of servo drives with a flexible coupling using a modified luenberger observer," in *Proc. 41st Annu. Conf. IEEE Ind. Electron. Soc. (IECON)*, Nov. 2015, pp. 1103–1108.

[22] Z.-G. Yin, C. Zhao, Y.-R. Zhong, and J. Liu, "Research on robust performance of speed-sensorless vector control for the induction motor using an interfacing multiple-model extended Kalman filter," *IEEE Trans. Power Electron.*, vol. 29, no. 6, pp. 3011–3019, Jun. 2014.

[23] R. Panigrahi and B. Subudhi, "Performance enhancement of shunt active power filter using a Kalman filter-based H_∞ control strategy," *IEEE Trans. Power Electron.*, vol. 32, no. 4, pp. 2622–2630, Apr. 2017.

[24] F. Auger, M. Hilairet, J. M. Guerrero, E. Monmasson, T. Orlowska-Kowalska, and S. Katsura, "Industrial applications of the Kalman filter: A review," *IEEE Trans. Ind. Electron.*, vol. 60, no. 12, pp. 5458–5471, Dec. 2013.

[25] H. Ji, S. Wang, and S. Huang, "Research of permanent magnet servo system based on disturbance observer and Kalman filter," in *Proc. 35th Chin. Control Conf. (CCC)*, Jul. 2016, pp. 4471–4475.

[26] N. K. Quang, N. T. Hieu, and Q. P. Ha, "FPGA-based sensorless PMSM speed control using reduced-order extended Kalman filters," *IEEE Trans. Ind. Electron.*, vol. 61, no. 12, pp. 6574–6582, Dec. 2014.

[27] X. Xiao and C. Chen, "Reduction of torque ripple due to demagnetization in PMSM using current compensation," *IEEE Trans. Appl. Supercond.*, vol. 20, no. 3, pp. 1068–1071, Jun. 2010.

[28] S. Wang, W. Zhu, J. Shi, H. Ji, and S. Huang, "A high performance permanent magnet synchronous motor servo system using predictive functional control and Kalman filter," *J. Power Electron.*, vol. 15, no. 6, pp. 1547–1558, Nov. 2015.

[29] P. Tety, A. Konaté, O. Asseu, E. Soro, and P. Yoboué, "An extended sliding mode observer for speed, position and torque sensorless control for PMSM drive based stator resistance estimator," *Intell. Control Autom.*, vol. 7, no. 1, pp. 1–8, 2016.

[30] C. Lin, A. Dong, and J. Shi, "Dynamic smoothness control for dual-motor-independent-drive electric vehicles based on Kalman filter," *Energy Procedia*, vol. 88, pp. 1005–1012, Jun. 2016.

[31] B. Ekstrand, "Poles and zeros of α-β and α-β-γ tracking filters," *IEE Proc. D, Control Theory Appl.*, vol. 148, no. 5, pp. 370–376, 2001.

[32] T. Benedict and G. Bordner, "Synthesis of an optimal set of radar track-while-scan smoothing equations," *IRE Trans. Autom. Control*, vol. 7, no. 4, pp. 27–32, Jul. 1962.

[33] D. F. Crouse, "A general solution to optimal fixed-gain (α-β-γ etc.) filters," *IEEE Signal Process. Lett.*, vol. 22, no. 7, pp. 901–904, Jul. 2015.

[34] B. Friedland, "Optimum steady-state position and velocity estimation using noisy sampled position data," *IEEE Trans. Aerosp. Electron. Syst.*, vol. AES-9, no. 6, pp. 906–911, Nov. 1973.

[35] X. Cai, C. Wang, and R. Kennel, "A fast and precise grid synchronization method based on fixed-gain filter," *IEEE Trans. Ind. Electron.*, vol. 65, no. 9, pp. 7119–7128, Sep. 2018.

[36] A. Bellini, S. Bifaretti, and F. Giannini, "A robust synchronization method for centralized microgrids," *IEEE Trans. Ind. Appl.*, vol. 51, no. 2, pp. 1602–1609, Jul. 2014.

CAN WANG received the B.S. degree in electrical engineering from the Harbin University of Science and Technology, Harbin, China, in 2012, and the M.S. and Ph.D. degrees in power electronics and electrical drives from the Harbin Institute of Technology, in 2014 and 2019, respectively. In 2017, she was with the EAL Research Group, Technical University of Munich, Germany, on the one-year CSC Project. She is currently working as an Assistant Professor with the College of Mechatronics and Control Engineering, Shenzhen University. Her research interests include PMSM servo systems, motor drive control, and mechanical resonance suppression.

WEINAN WU received the B.S. degree in electrical engineering from the Harbin University of Science and Technology, Harbin, China, in 2010, and the M.S. degree from the College of Intelligent Systems Science and Engineering, Harbin Engineering University, Harbin, in 2013, where he is currently pursuing the Ph.D. degree. He is working with the Beijing Institute of Specialized Machinery. His research interests include control science and engineering and servo drive control.

GUOCHONG LI received the B.S. degree in automation from Shenzhen University, in 2017. He is currently pursuing the master's degree with the College of Mechatronics and Control Engineering, Shenzhen University. His research interests include motor control, PMSM systems, and coordinated position control.

GUILIN YANG (Member, IEEE) received the B.S. and M.S. degrees from the Jilin University of Technology, China, in 1985 and 1988, respectively, and the Ph.D. degree from Nanyang Technological University, Singapore, in 1999. From 1998 to 2013, he was a Scientist, a Senior Scientist, and the Manager of the Mechatronics Group, Singapore Institute of Manufacturing Technology, Singapore. Since 1988, he has been a Lecturer, the Division Head, and the Vice Dean of the School of Mechanical Engineering, Shijiazhuang Railway Institute, China. He joined the Ningbo Institute of Material Technology and Engineering, Chinese Academy of Sciences, China, in 2013, where he is currently a Professor and the Vice-President. He has published more than 280 technical papers in referred journals and conferences. His current research interests include precision actuators, parallel-kinematics machines, modular robots, cable-driven manipulators, and industrial robots. He is also an Associate Editor of IEEE Access.

CHI ZHANG (Senior Member, IEEE) received the bachelor's and master's degrees from Xi'an Jiaotong University, in 1999 and 2002, respectively, and the Ph.D. degree from Nanyang Technological University, Singapore. From 2002 to 2005, he carried out the study and research work based on the design and control of disk-shaped magnetic levitation motor flywheel energy storage system with Nanyang Technological University. From 2005 to 2010, he worked with the ASM Technology Research and Development Center Singapore, the Dyson Research and Development Center, Singapore, and the Seagate Technology International Singapore Research and Development Center. In 2012, he joined the Ningbo Institute of Material Technology and Engineering, Chinese Academy of Sciences, as a Team Talent Researcher, where he engaged in the research of precision motion systems and control technology.

JIANFEI PAN (Member, IEEE) received the Ph.D. degree from the Department of Electrical Engineering, The Hong Kong Polytechnic University, Hong Kong, in 2006. He is currently working as a Professor with the College of Mechatronics and Control Engineering, Shenzhen University, Shenzhen, China. His main research interest includes design and control of linear motors and generators.